Instruments and Methods

Airborne radar sounder for temperate ice: initial results from Patagonia

Rodrigo ZAMORA,[1] David ULLOA,[1] Gonzalo GARCIA,[1,2] Ronald MELLA,[1] José URIBE,[1] Jens WENDT,[1†] Andrés RIVERA,[1,3,4] Guisella GACITÚA,[1*] Gino CASASSA[1]

[1]*Centro de Estudios Científicos, Av. Arturo Prat 514, Casilla 1469, Valdivia, Chile*
E-mail: rzamora@cecs.cl
[2]*Dirección de Proyectos Investigación y Desarrollo de la Armada de Chile, General del Canto 398, Playa Ancha, Valparaíso, Chile*
[3]*Centro de Ingeniería de la Innovación del CECS (CIN), Av. Arturo Prat 514, Casilla 1469, Vadivia, Chile*
[4]*Departamento de Geografía, Universidad de Chile, Portugal 84, Casilla 3387, Santiago, Chile*

ABSTRACT. We describe the development of a low-frequency airborne radar specifically designed for the sounding of temperate ice. The system operates at a central frequency of 1 MHz and consists of an impulse transmitter with an output voltage up to 5000 V and a digital receiver with a maximum gain of 80 dB. The radar was deployed on board a CASA 212 aircraft, which also carries a laser altimeter, an inertial navigation system, a digital camera and a GPS receiver. A description of the radar system is provided, as well as preliminary results obtained at Glaciar Tyndall, Campo de Hielo Sur (Southern Patagonia Icefield), where an ice depth of 670 m was reached.

INTRODUCTION

Radio-echo sounding is a convenient method for determining ice thicknesses, internal reflections and bed properties (Plewes and Hubbard, 2001). Airborne radar systems are much more efficient than ground approaches, due to the comparatively more extensive surveyed areas, shorter survey times and safer operation over crevassed areas. In spite of the above, considerations of cost, logistics and flight safety must be taken into account when designing airborne radar systems, particularly when the hanging of dragged antennae is involved, as in the system presented here.

In polar regions, airborne radio-echo sounding has been the main method for determining ice thickness during recent decades, among other reasons, because cold ice is transparent to radio waves in a wide frequency spectrum, from 1 MHz to 10 GHz (e.g Bogorodsky and others, 1985). For example, in Antarctica ice thicknesses of nearly 5 km have been measured with ice radars (Plewes and Hubbard, 2001). In contrast, as ice approaches the melting point, attenuation losses increase substantially. For example, Glen and Paren (1975) found a six-fold increase in two-way attenuation in ice at –3°C compared with colder ice at –23°C, with values of 1.9 and 0.3 dB km^{-1}, respectively.

A major obstacle to electromagnetic wave propagation through temperate ice is the presence of englacial meltwater. Meltwater can result in water bodies with characteristic dimensions larger than 1 m (Watts and England, 1976). These bodies produce strong scattering of the electromagnetic waves at wavelengths smaller than the characteristic dimension of the water bodies. Scattering from surface crevasses is another major obstacle to the penetration of electromagnetic waves (Plewes and Hubbard, 2001). Therefore, at least theoretically, electromagnetic waves have a better possibility of penetrating through temperate and crevassed ice at frequencies smaller than ~5 MHz (Watts and England, 1976).

Here we present an airborne radar system for temperate ice designed at Centro de Estudios Científicos (CECS), Valdivia, Chile, which was successfully tested on Glaciar Tyndall, Campo de Hielo Sur (Southern Patagonia Icefield).

A REVIEW OF RADAR SOUNDING OF TEMPERATE GLACIERS

Successful ground-based radar surveys for detecting the ice thickness and internal stratigraphy of glaciers have been performed on temperate glaciers around the world following the basic design proposed by Watts and England (1976). These radar systems have operated at medium and high frequencies (MF/HF) of 1–10 MHz and generally have resistively loaded dipole antennae which follow the so-called Wu and King pattern (Wu and King, 1965). In Alaska, USA, a maximum depth of 600 m was penetrated on Taku Glacier by Nolan and others (1995), and of 630 m on Black Rapids Glacier by Gades (1998). In Patagonia, Raymond and others (2005) reported a maximum depth of 740 m at Glaciar Tyndall, and Rivera and Casassa (2002) reported a maximum depth of 750 m at Paso de los Cuatro Glaciares. In contrast, depths of >2.5 km have been sounded in cold ice with similar radar configurations in the Antarctic ice sheet (Jacobel and Welch, 2005). Gravity measurements performed over the Patagonian icefields (Casassa, 1987) show that ice thicknesses in excess of 1500 m can be expected. In spite of these ground measurements, ground radar systems have proven not to be practical for surveying the large icefields in Alaska and Patagonia.

Only a few airborne radar surveys over temperate ice have been carried out so far. Watts and Wright (1981) performed pioneering studies at Columbia Glacier, Alaska,

†Deceased.
*Present address: Natural Environmental Research Institute, Department of Arctic Environment, University of Aarhus, Frederiksborgvej 399, DK-4000 Roskilde, Denmark.

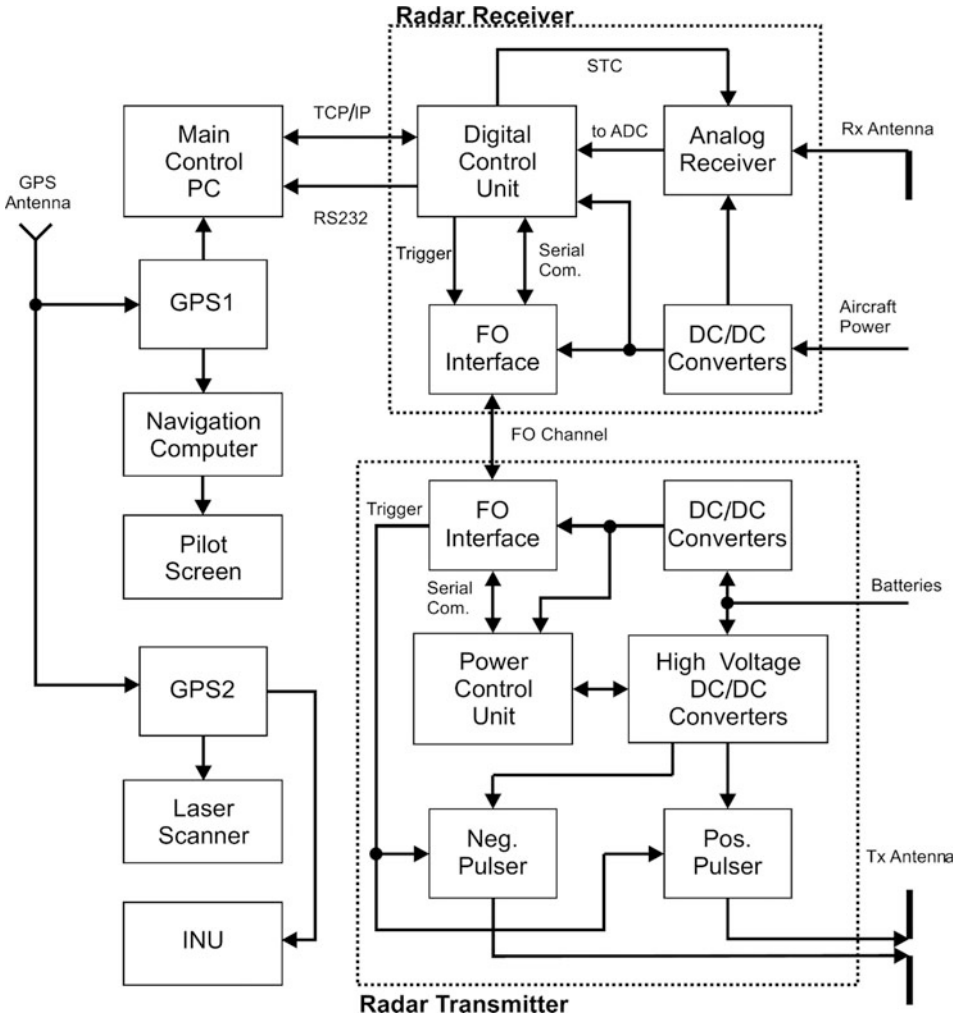

Fig. 1. Block diagram of the SIRAHT system, composed of a high-frequency impulse radar, a navigation system and a laser scanner altimeter (lidar). The upper unit is the receiver module that communicates with the computer system controlling the radar, which receives the digitized data. The receiver is connected to the transmitter unit through a fiber-optic cable transmitting synchronizing pulses.

being able to detect maximum ice thicknesses of 550 m They used a 1.2 MHz radar system, stringing the antennae around the wings of a Pilatus Porter aircraft. Kennett and others (1993) measured maximum thicknesses of 350 m at Svartisen ice cap, Norway, with a helicopter-borne impulse radar system operating at 8 MHz. After realizing the shortcomings of existing ground radars and based on earlier experiences, collaborative efforts have been recently undertaken in Alaska with two different impulse radar systems, one from the NASA Jet Propulsion Laboratory (JPL; personal communication from E. Rignot, 2008), and the other from the University of Washington, USA, (Conway and others, 2009) reaching maximum depths in excess of 1 km at some sites. In Patagonia, joint experiments were undertaken with the JPL airborne radar (personal communication from E. Rignot, 2008) and the SIRAHT (Spanish acronym for Airborne Radar System for Temperate Ice) described below.

In Patagonia, several experiments with airborne radars have been performed over Glaciar Tyndall. In 1999, a 150 MHz impulse radar system from the German Federal Institute of Geosciences and Natural Resources (BGR; Damm, 2004) was installed on board a helicopter, with the antennae transported as a hanging load (Casassa and others, 2001). In 2001, a 60 MHz ice-penetrating radar designed at the Technical University of Denmark (Christensen and others, 2000) was installed on board a Twin Otter aircraft (Keller and others, 2007), and in 2002 a 150 MHz coherent pulse compression radar from the University of Kansas, USA, (Gogineni and others, 1998) was installed on board a Chilean Navy P3 aircraft which flew over the Patagonian icefields (Casassa and others, 2003). Each of these systems was originally designed for the polar regions, and the results from Patagonia did not show any bed reflections. This is not surprising considering their relatively high frequencies, suggesting that the radar signals are effectively attenuated by the temperate ice, and also reflected and scattered by the abundant supraglacial and englacial water found in Patagonian glaciers.

SYSTEM DESCRIPTION

The problems associated with sounding glaciers using airborne methods in Patagonia prompted CECS in collaboration with the Chilean Navy to develop the SIRAHT instrument designed specifically for probing deep temperate glacial ice. We required the radar to have a low central frequency (~1 MHz), a high output power capability, and a receiver unit with high sensitivity.

The SIRAHT radar system is based on the design described by Watts and Wright (1981; Fig. 1). The complete

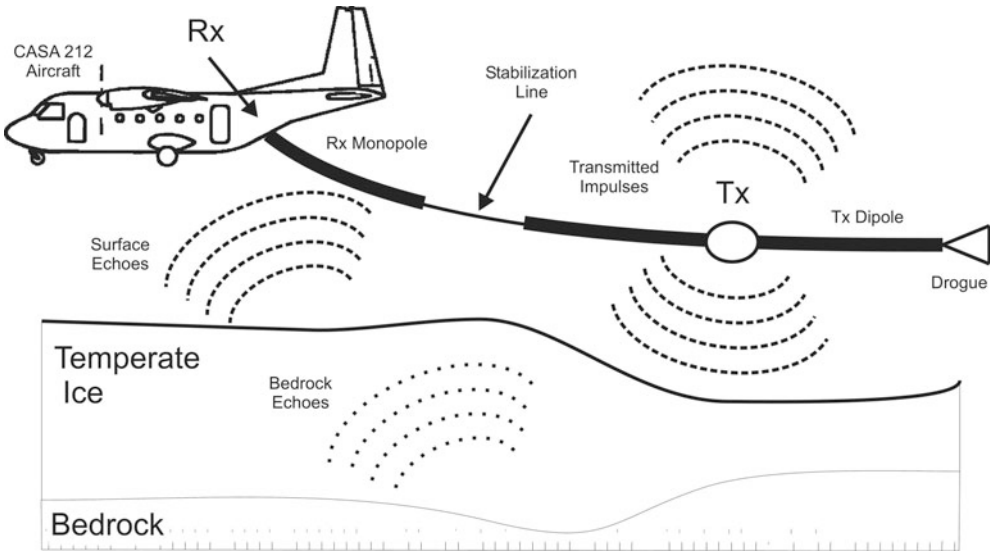

Fig. 2. Sketch of the radar deployment using the CASA 212 aircraft. Rx is the receiver and Tx is the transmitter.

system contains a MF/HF impulse radar, a suitable navigation system and a laser scanner system (lidar).

SIRAHT uses a bi-static configuration. The design of the transmitting and receiving antennae utilizes the Wu and King (1965) resistive load pattern to reduce oscillations, with a total impedance of 1200 Ω. The transmitter is a dipole with a length of 75 m for each arm, while the receiver is an 80 m long monopole antenna which is grounded to the aircraft. The antenna separation between the end of the receiving monopulse and the end of the transmitting dipole is 50 m. This configuration allows the receiver, processor and recorder to be installed inside the airplane, with the disadvantage that the received radiation pattern is asymmetrical since the aircraft produces distortions in the diagram of radiation and also increases the ringing.

The theoretical central frequency of the system is 1 MHz. Operating at these low frequencies involves the technical problem of dealing with large (several tens of meters) physical antenna dimensions. One reasonable solution, which was adopted in this project, is the deployment and towing of the antennae out of the aircraft during flight, similar to the procedure followed by Watts and Wright (1981). But unlike Watts and Wright, our antenna system was deployed at the rear of the aircraft, as described below (Fig. 2).

The transmitter is controlled via fiber optics to avoid direct electromagnetic coupling. The digital control unit generates a 400 ns pulse, which is sent through the fiber-optic cable to the transmitter. This pulse controls the on-state time of the four high-voltage MOSFETs (metal-oxide semiconductor field-effect transistors) and also controls the push–pull amplifier composed of transistors Q1, Q2 and Q3, which drive the transistor Q4, which is responsible for switching a pulse of 15 V in the primary of transformer T1 and T2 (Fig. 3). These transformers serve as a galvanic insulation circuit between the low-voltage control and the high-voltage modulator. Each transformer drives the gate of two high-voltage MOSFETs. The Zener diodes located before each MOSFET protect the gate from dangerous voltage peaks, and their associated resistance decreases the ringing at the entrance of each transistor due to the short rising pulse time.

The four MOSFETs in a series configuration operate as a high-voltage switch (4 kV maximum), where each transistor is able to operate up to 1.1 kV. We have, therefore, two states: when the switch is open and when it is closed (Fig. 4a and b). In the off-state (most of the time), the capacitor C (2 nF) is slowly loaded with the voltage of the source of high voltage through the resistor R (20 kΩ) and the diode D, the latter in forward bias during this period. When the switch changes to the on-state, the D diode changes to a reverse bias condition, and then the fully loaded capacitor discharges quickly through the load (antenna). Given the short duration of this state (400 ns), when the switch opens, putting the diode in a forward bias condition and thus isolating the antenna, the capacitor still has remaining storage energy, which does not discharge into the load. Table 1 illustrates the basic radar parameters.

The transmitter module receives power from an external source in the range 24–36 V dc. A series connection of two 12 V, 7 Ah batteries was installed for this test flight, providing 2.5 hour battery life. The transmitter (inside a fiberglass case) weighs 20 kg and can operate at temperatures as low as –30°C.

The receiver subsystem has a dynamic range of 80 dB, including the use of a sensitivity time control (STC). The STC time function is generated by the digital control unit using a digital–analog converter (DAC) THS5661A at 50 MHz sampling rate which can be modified by software. The STC has a control voltage (–5 to 0 V) which manages simultaneously two MMIC attenuators (HMC346) located in the low-noise amplifier (LNA). Each attenuator has an attenuation range of 32 dB, resulting in a total STC dynamic range of 64 dB. The receiver has a bandwidth of 700 kHz to 7 MHz, a sampling rate of 100×10^6 samples s^{-1} and a resolution of 12 bits.

The matching impedance of the receiving antenna was obtained using a broadband ferrite UNUN transformer (UN-B-800-612-450, CWS BiteMark, Inc.), adapting from 800 Ω to the standard 50 Ω impedance (the receiver input impedance). All data are stored on a PC together with global positioning system (GPS) position information.

The navigation system uses a GPS receiver, which sends NMEA (US National Marine Electronics Association) data to a computer running dedicated software, which processes position, speed and aircraft heading, and generates real-time mapping feeding a very high-frequency omnirange (VOR)-

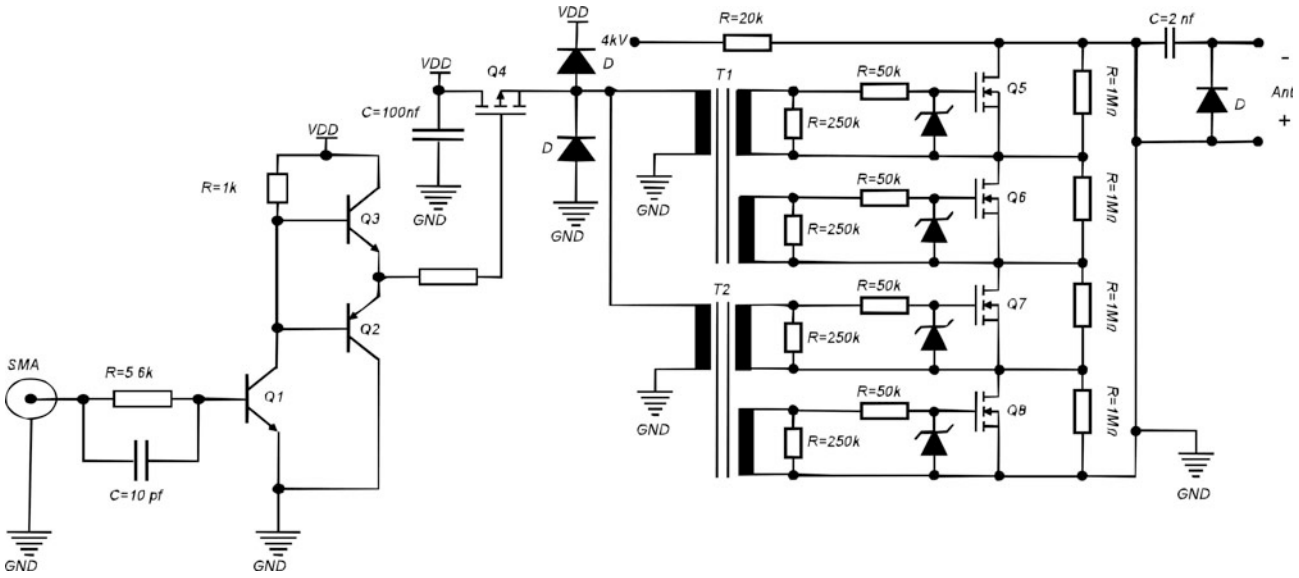

Fig. 3. Transmitter power circuit schematic of negative pulser. Upper left ports are used for the high-voltage power supply, lower left ports command the impulse instant and right ports correspond to the pulser output (complementary to the positive modulator).

type navigation instrument. The navigation data are viewed on a screen located in the aircraft's cockpit.

The lidar system has its own GPS receiver which sends NMEA and pulse per second (PPS) signals to the laser scanner and to the inertial navigation system (INS) for recording the aircraft trajectory. Kinematic GPS solutions are computed differentially using two Javad Lexon GD receivers, one installed on the aircraft and another on the ground as reference station.

A CASA 212 aircraft of the Chilean Navy is used for flying the system, mainly because its back ramp can be opened during flight to deploy the antennae. The antennae deployment process has two stages: first, a stabilization line is uncoiled by means of a hydraulic winch; then the antennae plus transmitter are fixed along the stabilization line using a manual winch, attaching the two transmitter dipoles and one receiver monopole to the stabilization line by means of small carabiners. A 2 m long drogue is attached to the end of the stabilization line to reduce wagging. The receiving monopole dipole is grounded to the aircraft, being dragged immediately behind the back ramp. The transmitter is housed inside an aerodynamic fiberglass casing which is 2 m long, located 250 m behind the aircraft, in the centre of the transmitting antenna. The set-up is approved by the Chilean Navy Aviation. Figure 2 shows the system deployment.

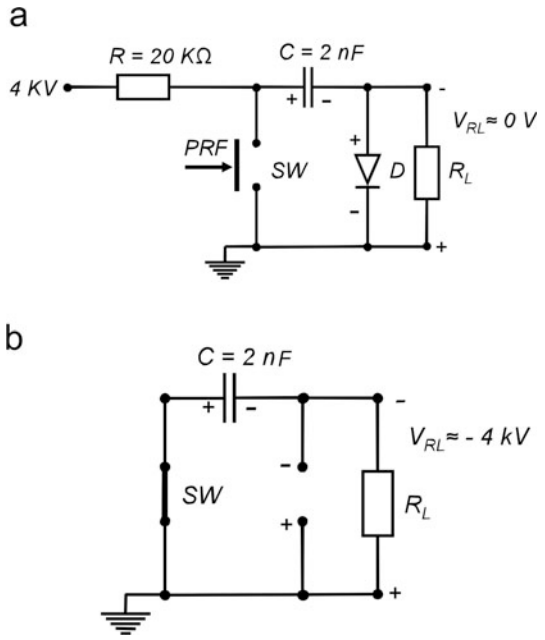

Fig. 4. Simplified schematic of the MOSFET configuration representing an open (a) and closed (b) switch of the negative modulator (complementary to the positive modulator).

RESULTS FROM A FIELD TEST IN PATAGONIA

Tests over sea water were performed on 27 November 2006, over Bahía Inútil, Straits of Magellan, ~50 km east of the city of Punta Arenas, to calibrate the system. On 4–5 December 2006 two flights were conducted over Glaciar Tyndall. The glacier flights included two longitudinal loops, each with a length of ~40 km. Both loops started at the glacier front (~100 m a.s.l.), reached a maximum elevation of ~800 m a.s.l. in the ablation area and returned, through a

Table 1. System specifications

Tx impulse voltage	0–6 kV
Pulse rise time	<40 ns
Pulse fall time	1 μs into 300 Ω
Tx pulse width	500 ns
Pulse-repetition frequency	Selectable up to 5 kHz
Power supply	18–36 V dc
Central frequency	1 MHz
Rx bandwidth	700 kHz to 7 MHz
Tx peak power	20 kW
Minimum detectable signal	–102 dBm (bandwidth 1 MHz)
Rx dynamic range	80 dB with STC
Sampling rate	100×10^6 samples s^{-1}, 12 bit

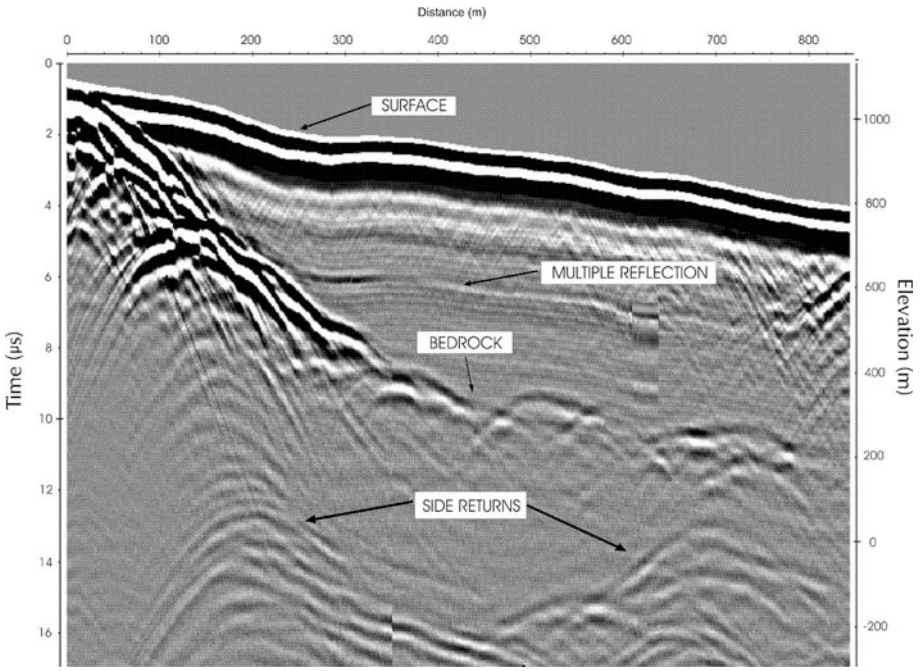

Fig. 5. Radargram recorded at Glaciar Tyndall using the SIRAHT airborne radar system. The two-way travel time (ordinate axis) is converted to depths using a radio-wave speed of 169 m (Conway and others, 2009). Mean subtraction of a dewow filter (used to eliminate a low-frequency component common to GPR systems; 1 μs), a mean filter in the time domain (five samples) and a background removal restricted to the noisiest sample range between 3.7 and 4.3 μs have been applied to the raw data.

different track, to the glacier front. During flights the mean height above the ground was ~400 m and the mean air speed was 100 knots (185 km h^{-1}).

Two-way travel times and amplitudes of the bed reflection wave were determined using specific software developed by CECS, and REFLEXW developed by K.J. Sandmeier (Germany). Data show bedrock returns in most of the echograms, indicating a rough subglacial topography (Fig. 5). Multiple side returns from surface topography are also detected in the radar echograms because of the nature of the dipole antenna which captures backscattering radiation originating from the surrounding surface topography. In order to discriminate the bedrock signal from the side returns, the recorded radar data were compared with simulated returns using surface topography data and the slopes of diffraction hyperbolae with REFLEXW and specific software developed by CECS. After discriminating bed returns from side returns, ice thicknesses of up to 600 m were detected (Fig. 5), with a maximum thickness of 670 m at 520 m a.s.l. near the glacier centre. The area covered by the airborne survey corresponds to the ablation area, composed of bare ice and completely free of snow at the time of the survey (end of the austral spring). Independent ground data collected previously with ice-penetrating radars on the middle to upper ablation area of Glaciar Tyndall (Casassa and Rivera, 1998; Godoi and others, 2003; Raymond and others, 2005) show very similar ice-thickness results, with differences from our data of less than ±50 m.

We interpret the radar clutter and hyperbolae within the glacier as observed in the radargram of Figure 5 (2–4 μs from the ice surface) to be caused by a combination of englacial water and surface crevasses. Except for a very few areas close to mountain tops, glaciers in Patagonia are temperate and as such have abundant supraglacial, englacial and subglacial water. Previous ground data we have collected with a 5 MHz system show very clear internal stratigraphy and bed returns down to 1300 m in the Antarctic interior (Casassa and others, 2004), while in Patagonia (Rivera and Casassa, 2002) our results show that internal stratigraphy and bed returns can only be detected down to 750 m at the most.

CONCLUDING REMARKS

The impulse radar, SIRAHT, detected temperate ice thicknesses up to 670 m, limited by the glacier geometry in the lower to middle ablation sectors of Glaciar Tyndall. The ice-thickness results are the first successful airborne measurements of ice depth in Patagonia. Inspection of the radar data shows a large number of side returns originating from off-axis surface topography features which can be confused with bed returns. Analysis of diffraction hyperbolae slopes and simulation of side returns based on the aircraft's tracks and a digital elevation model of the surface proved to be useful tools for discriminating side returns from bed echoes. This initial test shows the ability of the SIRAHT instrument to detect ice-thickness measurements in temperate ice, which opens new perspectives for the aerial mapping of temperate icefields, an essential task for characterizing the present state, and projecting the future evolution, of these ice masses. Further airborne surveys are planned in Patagonia, covering the ablation and accumulation areas of glaciers and exploring the maximum penetration depth of SIRAHT under different conditions.

ACKNOWLEDGEMENTS

The cooperation of the Chilean Navy, which provided the CASA 212 aircraft and its specialized crew, is acknowledged. We thank S. Lorimer and Linktronic for the radar design and construction. CECS is a non-profit organization funded in part by the Millennium Science Initiative and grants from Fundación Andes and the Tinker Foundation.

Institutional support to CECS from Empresas CMPC is gratefully acknowledged. CIN is funded by the Comisión Nacional de Investigación Cientifica y Tecnológica de Chile (CONICYT) and the Gobierno Regional de Los Rios. Comments from C. Fogwill and E. Rignot are appreciated.

REFERENCES

Bogorodsky, V.V., C.R. Bentley and P.E. Gudmandsen 1985. *Radioglaciology.* Dordrecht, etc., D. Reidel Publishing Co.

Casassa, G. 1987. Ice thickness deduced from gravity anomalies on Soler Glacier, Nef Glacier and the Northern Patagonia Icefield. *Bull. Glacier Res.* 4, 43–57.

Casassa, G. and A. Rivera. 1998. Sondaje de radar digital en el glaciar Tyndall, Patagonia. *An. Inst. Patagonia,* **26**, 129–135.

Casassa, G. *and 7 others.* 2001. Estudios glaciológicos en Patagonia y Chile central utilizando un sistema aerotransportado de radio eco sondaje. *An. Inst. Patagonia,* **29**, 25–44.

Casassa, G. *and 12 others.* 2003. Thinning of the Patagonian Icefields from recent laser altimetry, SRTM and earlier cartographic data. [Abstr. C11C-0821.] *Eos,* **84**(46), Fall Meet. Suppl.

Casassa, G., A. Rivera, C. Acuña, H.H. Brecher and H. Lange. 2004. Elevation change and ice flow at Horseshoe Valley, Patriot Hills, West Antarctica. *Ann. Glaciol.,* **39**, 20–28.

Christensen, E.L., N. Reeh, R. Forsberg, J.H. Jörgensen, N. Skou and K. Woelders. 2000. A low-cost glacier-mapping system. *J. Glaciol.,* **46**(154), 531–537.

Conway, H., B. Smith, P. Vaswani, K. Matsuoka, E. Rignot and P. Claus. 2009. A low-frequency ice-penetrating radar system adapted for use from an airplane: test results from Bering and Malaspina Glaciers, Alaska. *Ann. Glaciol.,* **50**(51), 93–97.

Damm, V. 2004. Ice thickness and bedrock map of Matusevich Glacier drainage system (Oates Coast). *Terra Antarct.,* **11**(1), 85–90.

Gades, A.M. 1998. Spatial and temporal variations of basal conditions beneath glaciers and ice sheets inferred from radio echo soundings. (PhD thesis, University of Washington.)

Glen, J.W. and J.G. Paren. 1975. The electrical properties of snow and ice. *J. Glaciol.,* **15**(73), 15–38.

Godoi, M.A., R. Carvallo and M. Arévalo. 2003. Condición actual del lóbulo Zapata Sur, en la zona de ablación del Glaciar Tyndall, mediante radio-ecosondeo sobre la superficie glaciar. *An. Inst. Patagonia,* **31**, 5–15.

Gogineni, S., T. Chuah, C. Allen, K. Jezek and R.K. Moore. 1998. An improved coherent radar depth sounder. *J. Glaciol.,* **44**(148), 659–669.

Jacobel, R.W. and B.C. Welch. 2005. A time marker at 17.5 kyr BP detected throughout West Antarctica. *Ann. Glaciol.,* **41**, 47–51.

Keller, K., G. Casassa and A. Rivera. 2007. Airborne laser altimetry survey of Glaciar Tyndall, Patagonia. *Global Planet. Change,* **59**(1–4), 101–109.

Kennett, M., T. Laumann and C. Lund. 1993. Helicopter-borne radio-echo sounding of Svartisen, Norway. *Ann. Glaciol.,* **17**, 23–26.

Matsuoka, K., R. Saito and R. Naruse. 2004. A novel backpackable ice-penetrating radar system. *J. Glaciol.,* **50**(168), 147–150.

Nolan, M., R.J. Motyka, K. Echelmeyer and D.C. Trabant. 1995. Ice-thickness measurements of Taku Glacier, Alaska, U.S.A., and their relevance to its recent behavior. *J. Glaciol.,* **41**(139), 541–553.

Plewes, L.A. and B. Hubbard. 2001. A review of the use of radio-echo sounding in glaciology. *Progr. Phys. Geogr.,* **25**(2), 203–236.

Raymond, C.F., T.A. Neumann, E. Rignot, K. Echelmeyer, A. Rivera and G. Casassa. 2005. Retreat of Glaciar Tyndall, Patagonia, over the last half-century. *J. Glaciol.,* **51**(173), 239–247.

Rivera, A. and G. Casassa. 2002. Detection of ice thickness using radio-echo sounding on the Southern Patagonia Icefield. *In* Casassa, G., F. Sepúlveda and R. Sinclair, *eds. The Patagonian icefields: a unique natural laboratory for environmental and climate change studies.* New York, Kluwer Academic/Plenum Publishers, 101–115.

Watts, R.D. and A.W. England. 1976. Radio-echo sounding of temperate glaciers: ice properties and sounder design criteria. *J. Glaciol.,* **17**(75), 39–48.

Watts, R.D. and D.L. Wright. 1981. Systems for measuring thickness of temperate and polar ice from the ground or from the air. *J. Glaciol.,* **27**(97), 459–469.

Wu, T. and R. King. 1965. The cylindrical antenna with nonreflecting resistive loading. *IEEE Trans. Antennae Propag.,* **13**(3), 369–373.

MS received 1 February 2008 and accepted in revised form 8 December 2008